ON THE FORMATION OF AMINES (RNH₂) AND THE CYANIDE ANION (CN⁻) IN ELECTRON-IRRADIATED AMMONIA–HYDROCARBON INTERSTELLAR MODEL ICES

Y. S. KIM[1] AND R. I. KAISER[1,2]

[1] Department of Chemistry, University of Hawaii at Manoa, Honolulu, HI 96822, USA; ralfk@hawaii.edu
[2] NASA Astrobiology Institute, University of Hawaii at Manoa, Honolulu, HI 96822, USA

ABSTRACT

The present laboratory study simulated cosmic-ray-induced grain chemistry of nitrogen-bearing organic molecules in interstellar and cometary ices. Model ices of ammonia (NH_3)–methane (CH_4) were prepared and irradiated at 10 K under contamination-free, ultrahigh vacuum conditions with energetic electrons generated in the track of galactic cosmic-ray particles. The radiolysis-induced processing of nitrogen-bearing molecules was then monitored on line and in situ by a Fourier transform infrared spectrometer and a quadrupole mass spectrometer during the irradiation phase and subsequent warm-up phases. The analogous processing was also achieved in ammonia (NH_3) and six hydrocarbon (C_nH_{2n+2}; $n = 1$–6) ices. The formation of cyanide anion (CN^-) was commonly observed in both ices at 10 K, the temporal column density fit of which traced back the involvement of methylamine (CH_3NH_2)-based intermediates. Traces of CH_3NH_2 were evident at about 110 K through thin ammonia matrices in sublimation. From the point of radiative transfer, we further constrain the formation mechanism of aminoacetonitrile (NH_2CH_2CN) on icy grains of Sgr B2(N) under a cosmic-ray-induced photon field.

Key words: astrobiology – astrochemistry – cosmic rays – ISM: individual objects (Sagittarius B2) – ISM: molecules – methods: laboratory

Online-only material: color figures

1. INTRODUCTION

Over the last few years, the formation of amines (RNH₂)—organic molecules carrying the amino (–NH₂) group—in the interstellar medium has received considerable attention due to the crucial role as reaction intermediates in astrobiologically important molecules such as amino acids (Holtom et al. 2005; Bossa et al. 2009; Lee et al. 2009). The rotational transitions of methylamine (CH_3NH_2), the simplest amine, were detected toward the Sgr B2 and Ori A molecular clouds by Kaifu et al. (1974, 1975) and Fourikis et al. (1974). More recently, a pair of extensive molecular line surveys confirmed the constituency of methylamine toward the Sgr B2(N) molecular core with a fractional abundance of as much as 10^{-7} relative to hydrogen (Turner 1991; Nummelin et al. 2000). Apponi et al. (2008) searched for the next member of amines, ethylamine ($C_2H_5NH_2$), in Sgr B2; an unsuccessful search determined upper limits of the column densities of $(1–8) \times 10^{13}$ cm^{-2} corresponding to fractional abundances reaching 10^{-11}. Most recently, three rotational transitions of the related cyanide anion (CN^-) were detected toward the carbon-rich star IRC+10216 (Agúndez et al. 2010). The abundance and line profiles were derived to suggest the CN^- formation in the binary reaction channel over the radiative electron attachment to the neutral cyano radical. In the grain surface chemistry of the interstellar and cometary world, the cyanide anion is renowned for playing a vital role in the Strecker-type synthesis of α-aminonitriles, with the recent example of aminoacetonitrile (NH_2CH_2CN) detected toward Sgr B2(N) (Belloche et al. 2008).

In the solar system, the detection of cometary and meteoritic amines was scarce and rather tentative until the *Stardust* mission to Comet 81P/Wild 2 brought the planetary relevance back to our solar system. During the flyby of the comet, an in situ mass analyzer on board the spacecraft recorded the dominant anion of cyanide (CN^-), as nitrogen-rich volatiles hit the silver sensor (Kissel et al. 2004). Subsequently, the identification of cometary glycine (NH_2CH_2COOH) in the samples returned to Earth further suggests that the species originate in dense interstellar clouds (Elsila et al. 2009; Glavin et al. 2008). In addition to glycine, the extracted samples contained high levels of cometary methyl- and ethylamine, as well as traces of β-alanine ($NH_2CH_2CH_2COOH$), providing evidence that energetic processing of the parent bodies containing ammonia mixed with methane (CH_4) or ethane (C_2H_6) could be potential precursors to these biomolecules (Glavin et al. 2008).

Despite the importance of amines and the related cyanide anion (CN^-) in the astrochemical and astrobiological evolution of the interstellar medium, little is known on their actual formation routes. Astronomers initially regarded methylamine (CH_3NH_2) as the terminal product of hydrogenation series of hydrogen cyanide (HCN; Equation (1); Dickens et al. 1997), due to the fact that it was the latest detected among the series (Kaifu et al. 1974, 1975; Fourikis et al. 1974). In the following years, Huntress & Mitchell (1979) proposed complex ion–molecule routes that incorporate mantle-formed ammonia (NH_3) in the radiative association reaction such as reactions (2) and (3). Herbst (1985), however, emphasized more competitive channels leading to the protonation of ammonia (NH_3), which were then adopted by Rodgers & Charnley (2001). Accordingly, Garrod et al. (2008) proposed a gas–grain warm-up model intended to match the fractional abundance (10^{-7}) of methylamine in Sgr B2(N); galactic cosmic-ray (GCR) particles were modeled into initiating methyl radicals (CH_3) from methane and amino radicals (NH_2) from ammonia on grain surfaces, which recombine diffusively to form methylamine during the warm-up phases (Equation (4)). The photolytic formation of gas-phase methylamine (Equation (4)) was in turn simulated in the laboratory (Gardner & McNesby 1980; Ogura et al. 1988):

$$HCN \xrightarrow{2H} H_2C = NH \xrightarrow{H_2/2H} CH_3NH_2 \qquad (1)$$

$$NH_3 + CH_3^+ \rightarrow CH_3NH_3^+ \qquad (2)$$

$$CH_3NH_3^+ + e^- \rightarrow CH_3NH_2 + H \qquad (3)$$

$$NH_2 + CH_3 \rightarrow CH_3NH_2. \qquad (4)$$
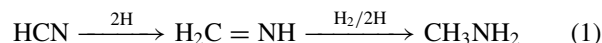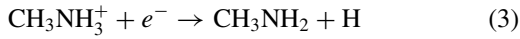
From the perspective of laboratory ice simulations, there has been lacking, if any, systematic studies to address the formation of amines and of the cyanide anion in low-temperature interstellar and solar system ices. To the best of our knowledge, Palumbo et al. (2000) were the pioneers who convincingly prepared and irradiated a mixture of ammonia (NH_3) and methane (CH_4) ices with 30 keV He^+ at 10 K. Using infrared spectroscopy, they tentatively assigned the newly formed species in irradiated ices to ethane (C_2H_6) at 2975 cm^{-1}, to a nitrile group (–C≡N) at about 2080 cm^{-1}, and to unknown species absorbing in 1800–1400 cm^{-1}. In particular, the weak absorption at 2080 cm^{-1} was reportedly persistent in solid phase up to 200 K. Previously in our group, we reported a series of experiments investigating the interaction of energetic electrons with ices of ammonia (Zheng et al. 2008) and methane (Bennett et al. 2006). The formation of the amino (NH_2) radical was traced at 1514 cm^{-1} (Equation (5)) and that of methyl radical (CH_3) at 608 and 3150 cm^{-1} (Equation (6)). The radical–radical recombination products of methyl and amino radicals, ethane (C_2H_6) and hydrazine (N_2H_4), respectively, were confirmed by the dual detection schemes: a Fourier transform infrared spectroscopy (FTIR) and a quadrupole mass spectrometry. Most recently, Zheng & Kaiser (2010) reported the formation of hydroxylamine (NH_2OH) in electron-irradiated ammonia (NH_3)–water (H_2O) ices via the radical–radical recombination of amino radicals with hydroxyl radicals (Equations (7) and (8)):

$$NH_3 \rightarrow NH_2 + H; \quad NH_2 + NH_2 \rightarrow N_2H_4 \qquad (5)$$

$$CH_4 \rightarrow CH_3 + H; \quad CH_3 + CH_3 \rightarrow C_2H_6 \qquad (6)$$

$$H_2O \rightarrow HO + H; \quad NH_3 \rightarrow NH_2 + H \qquad (7)$$

$$OH + NH_2 \rightarrow NH_2OH. \qquad (8)$$
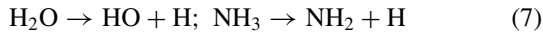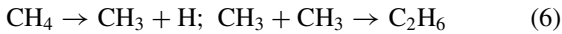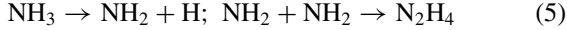
Herein, it is our primary interest to investigate to what extent amines (RNH_2) and cyanide anion (CN^-) will form in interstellar and cometary ammonia–hydrocarbon ices via cosmic-ray-induced radical–radical recombination (Equations (9)–(11)). For this purpose, we prepared interstellar and solar system model ices, ammonia (NH_3)–methane (CH_4) and ammonia (NH_3)–hydrocarbon mix C_nH_{2n+2} ($n = 1–6$), and subjected them to an ionizing interaction in the form of energetic (5 keV) electrons generated in the track of GCR particles (Bennett et al. 2005). We then aim to test whether the reaction sequence (Equations (9)–(11)) can lead to the formation of amines and possibly related compounds at temperatures as low as 10 K:

$$RH \rightarrow R + H \qquad (9)$$

$$NH_3 \rightarrow NH_2 + H \qquad (10)$$

$$R + NH_2 \rightarrow RNH_2. \qquad (11)$$
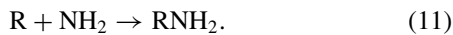
2. EXPERIMENTAL DETAILS

The experiments were conducted in an ultrahigh vacuum (UHV) chamber with a base pressure in the low 10^{-11} torr range (Bennett et al. 2004). Contamination-free vacuum conditions were rendered by a magnetically suspended turbo pump (1100 L s^{-1}) backed by an oil-free scroll pump. A differentially pumped rotary platform, which holds a highly polished silver

mirror as a substrate for the ice condensation, is positioned in the center of the chamber. Interfaced with the platform are a two-stage closed-cycle helium refrigerator (CTI Cryogenics) and a feedthrough for the programmable temperature controller (LakeShore 331). The temperature of the silver crystal can be regulated with a precision of ±0.3 K between 10 and 330 K. The gas mixture was prepared in a gas mixing chamber by the sequential addition of 9 mbar of NH_3 (99.99%; Matheson) and 500 mbar of hydrocarbon mix in helium (C_nH_{2n+2}, $n = 1–6$; 1000 ppm each; Matheson). The premixed gases were then deposited to the silver target at 10 K via a precision leak valve and a glass capillary array positioned 5 mm in front of the silver substrate. The deposition was carried out for 30 minutes at an inlet pressure of 4.0×10^{-7} torr. The mid-infrared spectra of solid samples were recorded from 6000 to 500 cm^{-1} with 4 or 2 cm^{-1} spectral resolution utilizing a Nicolet 6700 FTIR unit. The ammonia and methane (99.999%, Specialty Gas Group) gas mixture was analogously prepared and deposited to the substrate cooled at 10 K. The gas phase was monitored by a quadrupole mass spectrometer (Balzer QMG 420) operating in a residual gas analyzer mode with an electron impact ionization energy of 100 eV and a mass range of up to 200 amu.

Figure 1 depicts mid-infrared spectra of NH_3–CH_4 ices (a) and NH_3–hydrocarbon (C_nH_{2n+2}, $n = 1–6$) ices (b) recorded before (top) and after (bottom) irradiation with energetic electrons at 10 K. The vibrational assignments are compared with literature values in Table 1 (Socrates 2001; Bennett & Kaiser 2007; Bossa et al. 2008b). As demonstrated in both ice systems, our deposition conditions lead to a composite ice film, the infrared spectrum of which matches that of each individual component (Table 1). Notable in pristine NH_3–CH_4 ices were the CH_4 absorptions in the 2900–2600 cm^{-1} region, ν_1 in particular, while in NH_3–hydrocarbon ices were the group transitions of –CH_3/–CH_2– at about 2900, 1400, and 700 cm^{-1} (Figure 1; Bohn et al. 1994). The column density (molecules cm^{-2}) of ammonia in the system of NH_3–hydrocarbon ices was estimated to be $(1.6 \pm 0.2) \times 10^{17}$ molecules cm^{-2} by utilizing an integrated absorption coefficient (1.7×10^{-17} cm $molecule^{-1}$) for the ν_2 mode at 1080 cm^{-1} (Muñoz Caro & Schutte 2003). This translates into an ice thickness of 67 ± 6 nm after taking into account a solid density of 0.69 g cm^{-3} (Bossa et al. 2008b). The corresponding column density and ice thickness of hydrocarbons were estimated to be $(6.5 \pm 0.7) \times 10^{16}$ molecules cm^{-2} and 62 nm (Kim & Kaiser 2010). Concerning the ice system of NH_3 and CH_4, the following column density and ice thickness were also estimated for use: $(2.6 \pm 0.3) \times 10^{17}$ molecules cm^{-2} and 105 nm for NH_3; $(6.1 \pm 2.1) \times 10^{17}$ molecules cm^{-2} and 313 nm for CH_4.

The pristine ices were then irradiated isothermally with 5 keV electrons at a nominal beam current of 0 (blank), 100 nA, and 1 μA. The electron beams were generated with an electron gun (Specs EQ 22–35) and scanned over the target area of 3.2 ± 0.3 cm^{-2} to avoid heating of the target. Note that actual extraction efficiency of the electron gun is stated to be 78.8%, thus correcting the fluence down to 1.8×10^{15} electrons cm^{-2} hitting the target, for example, at a nominal current of 1 μA over 20 minutes. The electron trajectories and energy loss in layers of the ice system were simulated using the CASINO code (Drouin et al. 2001). These calculations yield an averaged transmitted energy of the electrons at about 4.53 keV; this indicates that 470 eV per impinging electron were transferred to the ices of NH_3–hydrocarbon mix C_nH_{2n+2} ($n = 1–6$). This value corresponds to an average linear energy transfer (LET)
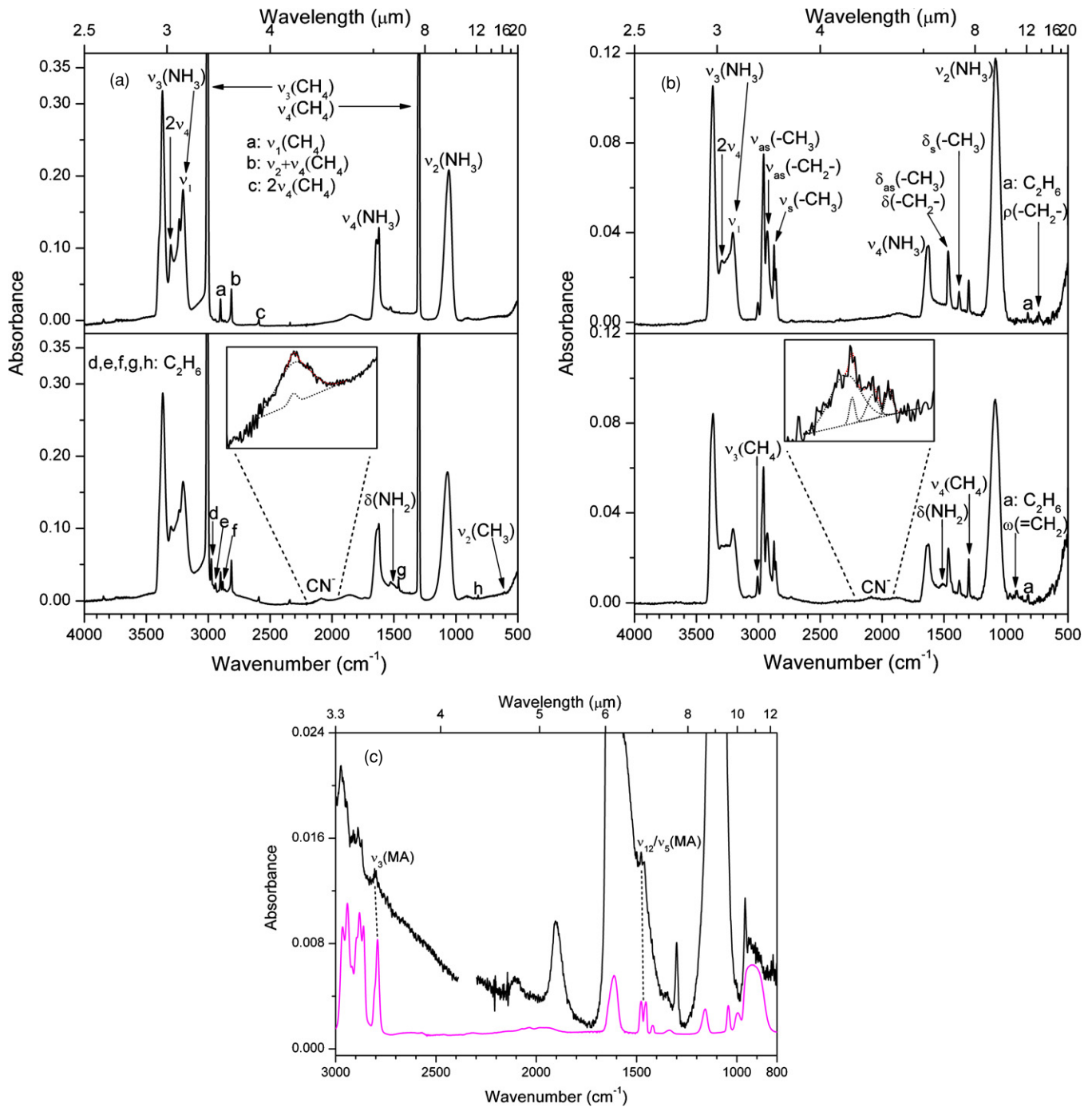
Figure 1. Mid-infrared spectra of ammonia (NH$_3$)–methane (CH$_4$) ice system (a) recorded before (top) and after (bottom) irradiation with 0.1 μA at 10 K. The inset shows the deconvoluted absorption of cyanide anion (CN$^-$) with Gaussians. System (b) depicts the analogous processing of ammonia (NH$_3$)–hydrocarbon (C$_n$H$_{2n+2}$; $n = 1$–6) ices with 1 μA at 10 K. The individual band assignments are compiled in Table 1. The black solid trace of panel (c) was recorded during warm-up phases at 113 K after system (a) was processed at 10 K, wherein the characteristic absorptions of methylamine (CH$_3$NH$_2$) are assigned and compared with an overview spectrum (magenta solid line) of reference CH$_3$NH$_2$ recorded at 10 K—refer to Section 3.1 for details. MA stands for methylamine.

(A color version of this figure is available in the online journal.)

of 3.6 keV μm^{-1}, on the order of magnitude that MeV cosmic rays typically transfer to an ice sample, i.e., a few keV μm^{-1} (Bennett et al. 2005). Therefore, the deposited ices receive an average dose of 3.8 $\pm$ 0.4 eV molecule^{-1} during 20 minute exposure at 1 μA. In the ice system of NH$_3$ and CH$_4$ were also achieved an LET of 3.1 keV μm^{-1} and a dose reaching 1.3 eV molecule^{-1} in up to a 90 minute exposure at 100 nA. After the irradiation, the ices are kept isothermally for 60 minutes before being heated to 300 K with a gradient of 0.5 K

minute^{-1}. This allows the sublimed molecules to be detected by the quadrupole mass spectrometer.

3. RESULTS

3.1. Infrared Spectroscopy

First, we will investigate the radiation-induced formation of new species in ammonia (NH$_3$)–methane (CH$_4$) ices. Figure 1(a) displays the infrared spectra of ices recorded at

Table 1
Infrared Absorption Features Recorded Before and After Irradiation of Both Ice Systems at 10 K: Ammonia (NH_3)–Methane (CH_4)
Ices and Ammonia (NH_3)–Hydrocarbon (C_nH_{2n+2}; $n = 1$–6) Ices

Irradiation at 10 K		Literature Assignment		
Before (cm^{-1})	After (cm^{-1})	Ref.	(cm^{-1})	Carrier
3369	. . .	1	3375	$\nu_3(NH_3)$
3296	. . .	1	3290	$2\nu_4(NH_3)$
3207	. . .	1	3210	$\nu_1(NH_3)$
3006	. . .	2	3011	$\nu_3(CH_4)$
. . .	2975[a]	3	2972	$\nu_{10}(C_2H_6)$
2958[b]	. . .	4	2975–2950	$-CH_3$ asym stretch
. . .	2941[a]	3	2941	$\nu_8+\nu_{11}(C_2H_6)$
2927[b]	. . .	4	2940–2915	$-CH_2-$ asym stretch
2901[a]	. . .	5	2904	$\nu_1(CH_4)$
. . .	2883[a]	3	2879	$\nu_5(C_2H_6)$
2874[b]	. . .	4	2885–2865	$-CH_3$ sym stretch
2860[b]	. . .	. . .	. . .	$-CH_2-$ sym stretch
2813[a]	. . .	5	2814	$\nu_2+\nu_4(CH_4)$
2591[a]	. . .	5	2593	$2\nu_4(CH_4)$
. . .	2089[a], 2088[a] 2087[b], 2081[b], 2056[b]	2	2083	$\nu(CN^-)$
. . .	2023[b]	6	2023	$\nu(N_3^-)$
1633	. . .	1	1625	$\nu_4(NH_3)$
. . .	1510	6	1514	$\delta(NH_2)$
1464[b]	1463[a] (C_2H_6)	3, 4	1465–1440	$-CH_3$ asym deform $-CH_2-$ scissor
1377[b]	. . .	4	1390–1370	$-CH_3$ sym deform
1302	. . .	2	1298	$\nu_4(CH_4)$
1081[b], 1061[a]	. . .	1	1075	$\nu_2(NH_3)$
. . .	911[b]	3, 4	911	$\omega(=CH_2)$
824[b]	821[a]	3	820	$\nu_{12}(C_2H_6)$
748[b], 732[b]	. . .	7	750–700	$-CH_2-$ rock
. . .	610[a]	8	608	$\nu_2(CH_3)$

Notes. Ninety minute irradiation (0.1 μA) of NH_3–CH_4 ices and 20 minute irradiation (1 μA) of NH_3–C_nH_{2n+2} ($n = 1$–6) ices both with 5 keV electrons; only new absorption features reported in irradiated ices at 10 K.
[a] Only with NH_3–CH_4 ices.
[b] Only with NH_3–C_nH_{2n+2} ($n = 1$–6) ices.
References. (1) Bossa et al. 2008b; (2) Moore & Hudson 2003; (3) Kim et al. 2010; (4) Socrates 2001; (5) Bennett & Kaiser 2007; (6) Zheng et al. 2008; (7) Bohn et al. 1994; (8) Bennett et al. 2006.

10 K before (top) and after (bottom) the irradiation at 0.1 μA. The radiation exposure at 10 K leads to multiple new absorption features. A list of carriers is identified and compiled along with the vibrational assignments in Table 1. A small but distinct level of amino (NH_2) and methyl (CH_3) radicals were observed in irradiated ices at 1510 cm^{-1} and 610 cm^{-1}, respectively. A set of new bands appearing at 2975, 2941, 2883, 1463, and 821 cm^{-1} were assigned to ethane (C_2H_6) in accord with the literature values (Kim et al. 2010). In fact, ethane was found to be the most abundant product in irradiated methane ices at 10 K (Bennett et al. 2006). The presence of hydrazine (N_2H_4) was not clear in irradiated ices at 10 K due to overlying absorptions of ammonia (NH_3), but it became clear during warm-up phases after ammonia had sublimed thoroughly from the substrate by 160 K (Zheng et al. 2008). Likewise, methylamine (CH_3NH_2) was pursued inconclusively at 10 K within the available spectral window where the detection could be unambiguous. The following spectral regions were aimed at about 2790 cm^{-1} for CH_3 stretch (ν_3) (Durig et al. 1968) and at about 1480/1460 cm^{-1} for the pair of CH_3 deformations (ν_{12}/ν_5) (Bossa et al. 2008a), also on account of the calibration that those CH_3 vibrations were found to least interact with coordinating matrices (Purnell et al. 1976). The detection proved to be a challenge even during warm-up phases, because CH_3NH_2

formed inside the matrix cage sublimed together with ammonia matrices. It was fortunate to monitor those CH_3NH_2 absorptions at about 110 K through thin ammonia matrices in sublimation (Figure 1(c)). This assignment is further corroborated in comparison with an overview spectrum of methylamine recorded as deposited at 10 K (Figure 1(c)); CH_3 stretches in the 3000–2700 cm^{-1} region bear closer resemblance than CH_3 deformations in the 1500–1400 cm^{-1} region do to their reference counterparts (Figure 1(c)); the 1460 cm^{-1} band at 110 K appears as a broad shoulder possibly blended in $-CH_3/-CH_2-$ transitions of unidentified traces, such as higher hydrocarbons (Kaiser & Roessler 1998) and ethylamine ($C_2H_5NH_2$) (Bernstein et al. 1995). Nonetheless, discretion has to be taken for interpreting those band profiles of highly interacting molecules such as CH_3NH_2 even further in different temperatures (Durig et al. 1968; Purnell et al. 1976; Bossa et al. 2008a).

The last species to mention is the carrier of a broad absorption at about 2088 cm^{-1} that developed during radiation exposure at 10 K and stayed persistent on the substrate up to about 160 K—the same feature Palumbo et al. (2000) observed in their ion-irradiated ices. The temporal evolution of this band is deconvoluted using Gaussians (see the inset of Figure 1) and then fit in first-order kinetic schemes. Cyanide anion (CN^-) is

assigned to this carrier at 10 K and higher temperatures. As a conjugate base of two isomers HCN/HNC, CN^- was previously found in irradiated nitrogen (N_2)–methane (CH_4) ices (Moore & Hudson 2003; Jamieson et al. 2009). It is worthwhile to note that a diagnostic stretch of nitriles (R–C≡N) was not evidenced even in a clear window of the 2200 cm^{-1} region (dello Russo & Khanna 1996), which precludes secondary destruction pathways.

Second, we will evaluate to what extent the ice processing may differ by substituting a mix of hydrocarbons (C_nH_{2n+2}, $n = 1$–6) for methane (CH_4) during radiation exposure at the higher emission (1 μA). At the expense of initial reactants, it permits the NH_2 radical and CN^- to evolve during the processing (Figure 1(b)). The inset also highlights the production of CN^- into three Gaussian components at 2087, 2081, and 2056 cm^{-1}, along with the new species at 2023 cm^{-1} attributable to azide (N_3^-) (Zheng et al. 2008; Table 1). Lastly, due to the radiolysis of heavier hydrocarbons (C_nH_{2n+2}, $n = 3$–6), a trace of alkenes appear at 911 cm^{-1}, along with the lighter products (C_nH_{2n+2}, $n = 1, 2$) resulting in the net increase in methane and ethane portions of Figure 1(b) (Kim & Kaiser 2010).

3.2. Mass Spectrometry

It is of interest to correlate the infrared observation with a mass spectroscopic analysis of the gas phase. The temporal evolution of individual reactants was traced at the corresponding molecular ion currents of ammonia (NH_3^+; $m/z = 17$) and six hydrocarbons ($C_nH_{2n+2}^+$; $n = 1$–6; $m/z = 16, 30, 44, 58, 72, 86$) released during warm-up phases after 0 (blank)/100 nA/ 1 μA irradiation of the ice mixture at 10 K (Kim & Kaiser 2010). Note that none of the newly formed species was detected in the residual gas analyzer during the actual irradiation phase, but only detected in the sublimation phases of the irradiated ices. In irradiated NH_3–CH_4 ices (0.1 μA), the ion current of $m/z = 30$ served to trace not only $C_2H_6^+$ released from solid ethane (C_2H_6) at about 80 K, but also $CH_2NH_2^+$, a mass fragment of methylamine ($CH_3NH_2^+$; $m/z = 31$), developed together with the ion current of ammonia (NH_3^+; $m/z = 17$) at about 110 K (Figure 2(a)). The individual ion current profiles are then compared to those previously reported in irradiated ices of pure ammonia (Figure 2(b); Zheng et al. 2008) and methane (Figure 2(c); Bennett et al. 2006). Surely, there were no such activities observed at 110 K in the individual ices as in the NH_3–CH_4 ices (Figure 2(a)), further strengthening our CH_3NH_2 assignment. Also referenced in Figure 2(d) is the sublimation profile of unirradiated methylamine with the maximum ion currents peaking at about 130 K. Meanwhile, in irradiated NH_3–C_nH_{2n+2} ($n = 1$–6) ices (1 μA), the amine (RNH_2) detection proved to be a challenge in that molecular ion currents ($C_nH_{2n+1}NH_2^+$; $n = 1$–6; $m/z = 31, 45, 59, 73, 87, 101$) fell below the detection limit. Even the detection of common amine fragments, $CH_2NH_2^+$ ($m/z = 30$) and $CH_3CHNH_2^+$ ($m/z = 44$), was hampered by high backgrounds set for $C_2H_6^+$ and $C_3H_8^+$ ion currents, respectively. Nonetheless, hydrazine ($N_2H_4^+$; $m/z = 32$) was monitored to sublime peaking at about 200 K.

4. DISCUSSION

In the current investigation, the cyanide anion (CN^-) was commonly found in the processing of NH_3–CH_4 and NH_3–C_nH_{2n+2} ices with energetic electrons at 10 K (Figure 1). This anion was also reported to be evident along with metha-
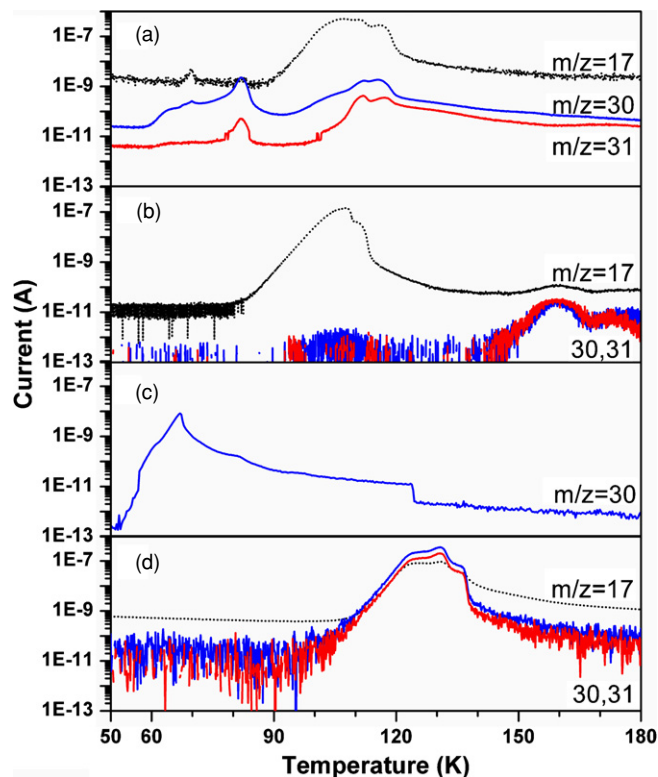
Figure 2. Temporal evolution of the ion currents of $m/z = 17$ (NH_3^+), 30 ($C_2H_6^+$/$CH_2NH_2^+$), and 31 ($^{13}C^{12}CH_6^+$/$CH_3NH_2^+$ during warm-up phases after the processing of NH_3–CH_4 ices (a) at 10 K. The ion current profiles are then compared in irradiated ices of ammonia (b) and methane (c); refer to Section 3.2 for details. Referenced in panel (d) are the mass fragments of unirradiated methylamine in sublimation after deposition at 10 K (Figure 1(c)). Traces are color-coded for clarity.

(A color version of this figure is available in the online journal.)

nimine (CH_2NH) in the processing of methylamine (CH_3NH_2) ice at 10 K (Bennett et al. 2010). *To what extent could methylamine be an intermediate in the formation of CN^-?* We set out to fit temporal profiles of CN^- column densities (A (CN^-) = 3.7×10^{-18} cm molecule^{-1}; Georgieva & Velcheva 2006) developed during radiation exposure at 10 K. Employing the consecutive A→B→C reaction scheme (12; Bennett & Kaiser 2005), we were able to fit the temporal evolution of CN^- in NH_3–CH_4 ices at 0.1 μA (Figure 3, top panel); also overlaid is a less satisfactory fit using one-step A→C reaction scheme (13). As schematically detailed in Figure 4, we formally consider A as the portion of NH_3–CH_4 ices that radiolyzes to form B (k_1), leading to C (k_2) of the cyanide anion (CN^-) formation. Three intermediates of B were considered to feed into the CN^- formation. The first intermediate to consider was the radiolysis-induced NH_2/CH_3 radical pair in the matrix cage, undergoing the facile radical–radical recombination to methylamine (CH_3NH_2) and further—via unimolecular decomposition of this reaction intermediate—to methanimine (CH_2NH) with a net loss of H_2/2H. On account of the non-detection of the HCN/HNC pair at 10 K (Figure 1), bulk ammonia was also considered as a base (Ba) for deprotonating HCN to CN^- in the CH_2NH decomposition pathway (Equations (14a) and (14b); Bennett et al. 2010):

$$[CN^-]_t = [A]_0 \left(1 - \frac{k_2}{k_2 - k_1} e^{-k_1 t} + \frac{k_1}{k_2 - k_1} e^{-k_2 t} \right) \quad (12)$$

$$[CN^-]_t = [A]_0 \left(1 - e^{-kt} \right) \quad (13)$$
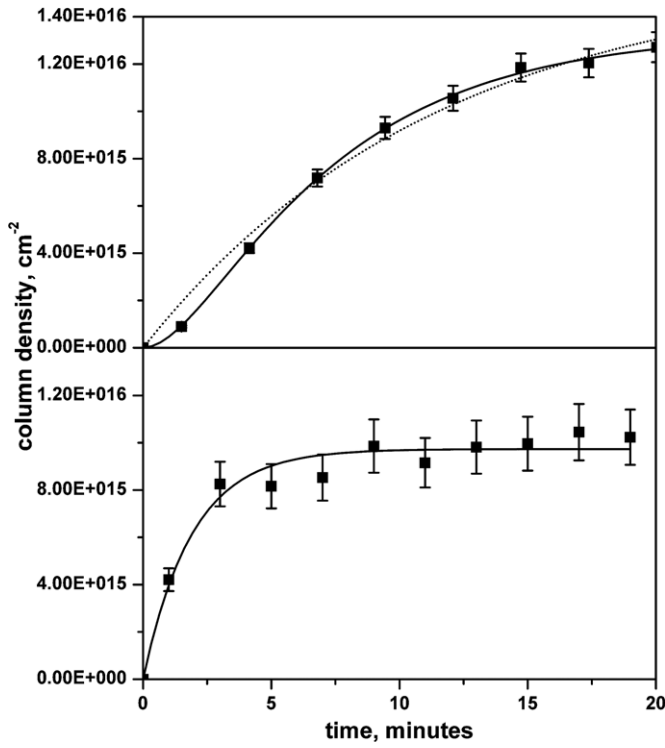
Figure 3. Fit of temporal cyanide (CN^-) column densities developed during radiation exposure of NH_3–CH_4 ices at 0.1 μA (top panel) and NH_3–C_nH_{2n+2} ($n = 1$–6) at 1 μA (bottom panel). Each profile is fit for comparison using consecutive A→B→C (solid line) and one-step A→C (dotted line) reaction schemes, even though both 1 μA fits are found to be indistinguishable.

$$CH_2NH \rightarrow HCN + H_2/2H \qquad (14a)$$

$$HCN + Base \rightarrow CN^- + HBase^+. \qquad (14b)$$
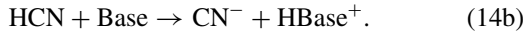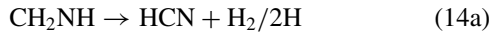
Note that none of these intermediates were observed in irradiated ices at 10 K, although individual, recombining NH_2 and CH_3 radicals yield CH_3NH_2 during warm-up phases as observed at about 110 K (Equation (4)). Attention was also paid to the three parameters of Equation (12) optimized through the fitting process. The initial fraction of NH_3–CH_4 ices, $A_0 = (1.3 \pm 0.0) \times 10^{16}$ molecules cm^{-2}, is about 5% the ammonia (NH_3) deposit, ultimately constraining the radiolysis-induced $[CN^-]_t$ by the two consecutive reaction rates of $k_1 = (2.7 \pm$
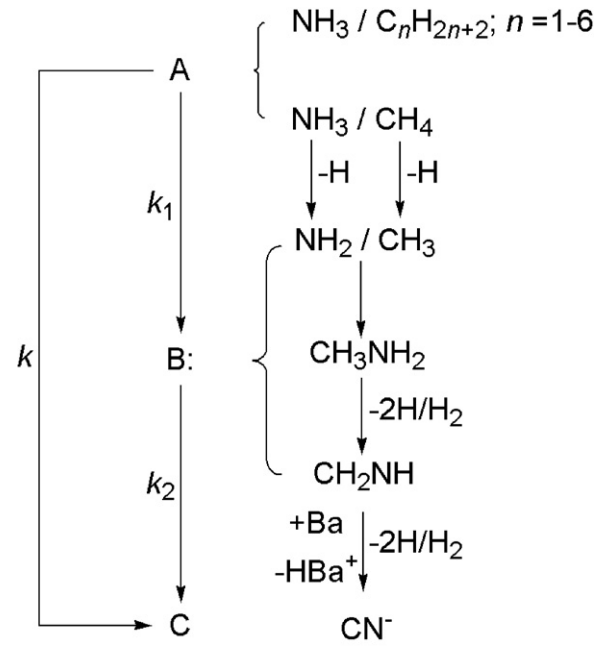
Figure 4. Reaction schemes of consecutive A→B→C and one-step A→C reactions. A stands for the portion of ice deposits that radiolyzes at 10 K to form a set of B intermediates leading to C of the cyanide anion (CN^-) formation; refer to Section 4 for details.

$0.3) \times 10^{-3}$ s^{-1} and $k_2 = (8.9 \pm 1.6) \times 10^{-3}$ s^{-1} (Table 2). The second step (k_2) is found to proceed three times faster than the first step (k_1), indicative of the nascent nature of the intermediates under ionizing radiation to yield CN^- as a stable product. Switching to NH_3–C_nH_{2n+2} ($n = 1$–6) ices with higher emission current (1 μA) enhanced the second step (k_2) to the level where the fit (solid line) of the consecutive A→B→C scheme becomes indistinguishable from that (dotted line) of the one-step A→C scheme with a pseudo first-order rate at $(8.7 \pm 1.3) \times 10^{-3}$ s^{-1} (Figure 3, bottom panel). Nonetheless, the initial fractions A_0 are derived to be $(1.0 \pm 0.0) \times 10^{16}$ molecules cm^{-2} after a normalization, or 4% the ammonia deposit, tracking the pathway of methylamine-based intermediates of B (Table 2).

5. ASTROPHYSICAL IMPLICATIONS

In this laboratory simulation, we have demonstrated cosmic-ray-induced grain ice chemistry of nitrogen-bearing organic

Table 2
Comparison of Rate Constants and Initial Concentrations Derived Using the Consecutive A→B→C and One-step A→C
Reaction Schemes to Fit the Temporal Evolution of Cyanide (CN^-) in Figure 3

k_1 (s^{-1})	k_2 (s^{-1})	A_0 (molecules cm^{-2})	Reaction Scheme
		NH_3–CH_4 ices with 0.1 μA	
$(2.7 \pm 0.3) \times 10^{-3}$	$(8.9 \pm 1.6) \times 10^{-3}$	$(1.3 \pm 0.0) \times 10^{16}$ (5%)[a]	A→B→C
$(1.4 \pm 0.2) \times 10^{-3}$	...	$(1.6 \pm 0.1) \times 10^{16}$ (6%)[a]	A→C
		NH_3–C_nH_{2n+2} ($n = 1$–6) with 1 μA	
$(8.7 \pm 1.3) \times 10^{-3}$	$\gg 1$[b]	$(1.0 \pm 0.0) \times 10^{16}$ (4%)[a]	A→B→C[b]
$(8.7 \pm 1.2) \times 10^{-3}$	...	$(1.0 \pm 0.0) \times 10^{16}$ (4%)[a]	A→C

Notes. Fluence of 2.0×10^{14} electrons cm^{-2} hitting the target over the initial 20 minute irradiation at 0.1 μA, while that of 1.8×10^{15} electrons cm^{-2} with the same period at 1 μA.
[a] Yield from $[NH_3]_0 = (2.6 \pm 0.3) \times 10^{17}$ molecules cm^{-2}; A_0 with 1 μA factored by 1.6.
[b] Pseudo first-order.

molecules (CHN) (Ehrenfreund & Charnley 2000; Rodgers & Charnley 2001; Garrod et al. 2008). The specific aim was set for detecting amines (RNH_2), methylamine (CH_3NH_2) in particular, and cyanide anion (CN^-) via ionizing interaction of energetic electrons with a pair of mantle-formed ice systems: ammonia (NH_3)–methane (CH_4) ices and NH_3–hydrocarbon (C_nH_{2n+2}, $n = 1$–6) ices. We observed the radiolysis-induced formation of CN^- at 10 K in both systems, the temporal column density fit of which traced back the involvement of CH_3NH_2-based intermediates (Figures 3 and 4). Methylamine was indeed monitored at about 110 K via our dual detection schemes, in situ IR spectroscopy (Figure 1(c)) and quadrupole mass spectrometry (Figure 2(a)). As currently simulated in the laboratory, CN^- is expected to form on icy grains of star-forming regions, such as Sgr B2(N), under the cosmic-ray-induced photon ($\sim$10 eV) field of 10^3 photons cm^{-2} s^{-1} (Ehrenfreund & Charnley 2000). As the radiolyzed icy grains warm up during protostellar switch-on phase (Garrod et al. 2008), CN^- is likely to mobilize and react with the neighboring methanimine ($CH_2 = NH$) intermediate in the presence of NH_4^+ (Equation (14b)). As the net reaction illustrates in reaction (15), it is the Strecker-type synthesis of aminoacetonitrile (NH_2CH_2CN) that Koch et al. (2008) postulated, which utilizes a chemical network built on two isomers of HCN/HNC and water (H_2O).

From the point of radiative transfer, we further constrain the formation level of $[CN^-]_t$ on icy grains of Sgr B2(N). According to our radiolysis at 10 K, $[CN^-]_t$ reached about 5% the ammonia (NH_3) deposit, when the energy deposition reached 2.5×10^{17} eV cm^{-2} in NH_3–CH_4 ices (Table 2). This radiation exposure is found to be equivalent to about 8×10^5 yr of exposure time for the icy grains in Sgr B2(N) with a warm-up timescale of 1×10^6 yr (Ehrenfreund & Charnley 2000; Garrod et al. 2008). Alternatively, the nascent $CH_2 = NH$ in matrices may encounter suprathermal (a few eV) hydrogen atoms generated from C–H bond cleavage of either the hydrocarbon reactant (Bennett et al. 2006; Kim et al. 2010) or the HCN intermediate during radiolysis as low as at 10 K (Equation (16)). The incipient CH_2NH_2 radical could then recombine with the CN radical to form NH_2CH_2CN (Equation (17)). In this way, the radiolysis-induced grain surface production and subsequent desorption mechanism may operate in Sgr B2(N), accounting for the fractional abundances of CH_3NH_2, CH_2NH, and NH_2CH_2CN determined within two orders of magnitude (Nummelin et al. 2000; Belloche et al. 2008):
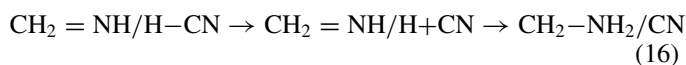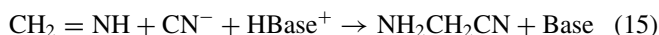
$$CH_2 = NH + CN^- + HBase^+ \rightarrow NH_2CH_2CN + Base \quad (15)$$

$$CH_2 = NH/H{-}CN \rightarrow CH_2 = NH/H{+}CN \rightarrow CH_2{-}NH_2/CN \quad (16)$$

$$CH_2NH_2 + CN \rightarrow NH_2CH_2CN. \quad (17)$$

REFERENCES

Agúndez, M., et al. 2010, A&A, 517, L2
Apponi, A. J., Sun, M., Halfen, D. T., Ziurys, L. M., & Müller, H. S. P. 2008, ApJ, 673, 1240
Belloche, A., Menten, K. M., Comito, C., Müller, H. S. P., Schilke, P., Ott, J., Thorwirth, S., & Hieret, C. 2008, A&A, 482, 179
Bennett, C. J., Jamieson, C. S., Mebel, A. M., & Kaiser, R. I. 2004, Phys. Chem. Chem. Phys., 6, 735
Bennett, C. J., Jamieson, C. S., Osamura, Y., & Kaiser, R. I. 2005, ApJ, 624, 1097
Bennett, C. J., Jamieson, C. S., Osamura, Y., & Kaiser, R. I. 2006, ApJ, 653, 792
Bennett, C. J., Jones, B., Knox, E., Perry, J., Kim, Y. S., & Kaiser, R. I. 2010, ApJ, 723, 641
Bennett, C. J., & Kaiser, R. I. 2005, ApJ, 635, 1362
Bennett, C. J., & Kaiser, R. I. 2007, ApJ, 660, 1289
Bernstein, M. P., Sandford, S. A., Allamandola, L. J., Chang, S., & Scharberg, M. A. 1995, ApJ, 454, 327
Bohn, R. B., Sandford, S. A., Allamandola, L. J., & Cruikshank, D. P. 1994, Icarus, 111, 151
Bossa, J.-B., Borget, F., Duvernay, F., Theulé, P., & Chiavassa, T. 2008a, J. Phys. Chem. A, 112, 5113
Bossa, J.-B., Duvernay, F., Theulé, P., Borget, F., d'Hendecourt, L., & Chiavassa, T. 2009, A&A, 506, 601
Bossa, J.-B., Theulé, P., Duvernay, F., Borget, F., & Chiavassa, T. 2008b, A&A, 492, 719
dello Russo, N., & Khanna, R. K. 1996, Icarus, 123, 366
Dickens, J. E., Irvine, W. M., DeVries, C. H., & Ohishi, M. 1997, ApJ, 479, 307
Drouin, D., Couture, A. R., Gauvin, R., Hovington, P., Horny, P., & Demers, H. 2001, Monte Carlo Simulation of Electron Trajectory in Solids (CASINO Version 2.42; Sherbrooke: Univ. Sherbrooke)
Durig, J. R., Bush, S. F., & Baglin, F. G. 1968, J. Chem. Phys., 49, 2106
Ehrenfreund, P., & Charnley, S. B. 2000, ARA&A, 38, 427
Elsila, J. E., Glavin, D. P., & Dworkin, J. P. 2009, Meteorit. Planet. Sci., 44, 1323
Fourikis, N., Takagi, K., & Morimoto, M. 1974, ApJ, 191, L139
Gardner, E., & McNesby, J. R. 1980, J. Photochem., 13, 353
Garrod, R. T., Weaver, S. L. W., & Herbst, E. 2008, ApJ, 682, 283
Georgieva, M. K., & Velcheva, E. V. 2006, Int. J. Quantum Chem., 106, 1316
Glavin, D. P., Dworkin, J. P., & Sandford, S. A. 2008, Meteorit. Planet. Sci., 43, 399
Herbst, E. 1985, ApJ, 292, 484
Holtom, P. D., Bennett, C. J., Osamura, Y., Mason, N. J., & Kaiser, R. I. 2005, ApJ, 626, 940
Huntress, W. T., Jr., & Mitchell, G. F. 1979, ApJ, 231, 456
Jamieson, C. S., Chang, A. H. H., & Kaiser, R. I. 2009, Adv. Space Res., 43, 1446
Kaifu, N., Morimoto, M., Nagane, K., Akabane, K., Iguchi, T., & Takagi, K. 1974, ApJ, 191, L135
Kaifu, N., Takagi, K., & Kojima, T. 1975, ApJ, 198, L85
Kaiser, R. I., & Roessler, K. 1998, ApJ, 503, 959
Kim, Y. S., Bennett, C. J., Chen, L.-H., O'Brian, K., & Kaiser, R. I. 2010, ApJ, 711, 744
Kim, Y. S., & Kaiser, R. I. 2010, ApJ, 725, 1002
Kissel, J., Krueger, F. R., Silén, J., & Clark, B. C. 2004, Science, 304, 1774
Koch, D. M., Toubin, C., Peslherbe, G. H., & Hynes, J. T. 2008, J. Phys. Chem. C, 112, 2972
Lee, C.-W., Kim, J.-K., Moon, E.-S., Minh, Y. C., & Kang, H. 2009, ApJ, 697, 428
Moore, M. H., & Hudson, R. L. 2003, Icarus, 161, 486
Muñoz Caro, G. M., & Schutte, W. A. 2003, A&A, 412, 121
Nummelin, A., Bergman, P., Hjalmarson, Å., Friberg, P., Irvine, W. M., Millar, T. J., Ohishi, M., & Saito, S. 2000, ApJS, 128, 213
Ogura, K., Migita, C. T., & Yamada, T. 1988, Chem. Lett., 17, 1563
Palumbo, M. E., Strazzulla, G., Pendleton, Y. J., & Tielens, A. G. G. M. 2000, ApJ, 534, 801
Purnell, C. J., Barnes, A. J., Suzuki, S., Ball, D. F., & Orville-Thomas, W. J. 1976, Chem. Phys., 12, 77
Rodgers, S. D., & Charnley, S. B. 2001, ApJ, 546, 324
Socrates, G. 2001, Infrared and Raman Characteristic Group Frequencies (3rd ed.; New York: Wiley)
Turner, B. E. 1991, ApJS, 76, 617
Zheng, W., Jewitt, D., Osamura, Y., & Kaiser, R. I. 2008, ApJ, 674, 1242
Zheng, W., & Kaiser, R. I. 2010, J. Phys. Chem. A, 114, 5251